Additive Manufacturing 18 (2017) 221–227

Contents lists available at ScienceDirect

Additive Manufacturing

journal homepage: www.elsevier.com/locate/addma

Full Length Article

Vacuum-filling of liquid metals for 3D printed RF antennas

Vivek Bharambe[a,1], Dishit P. Parekh[b,1], Collin Ladd[b], Khalil Moussa[c], Michael D. Dickey[b], Jacob J. Adams[a,*]

[a] Department of Electrical and Computer Engineering, North Carolina State University, Raleigh, NC 27695, USA
[b] Department of Chemical and Biomolecular Engineering, North Carolina State University, Raleigh, NC 27695, USA
[c] Materials and Process Development, 3D Systems, Rock Hill, SC, USA

ARTICLE INFO

Article history:
Received 4 April 2017
Received in revised form 23 August 2017
Accepted 8 October 2017
Available online 10 October 2017

Keywords:
3D printing
Liquid metals
Antennas
Vacuum filling
Microchannels

ABSTRACT

This paper describes a facile method to fabricate complex three-dimensional (3D) antennas by vacuum filling gallium-based liquid metals into 3D printed cavities at room temperature. To create the cavities, a commercial printer co-prints a sacrificial wax-like material with an acrylic resin. Dissolving the printed wax in oil creates cavities as small as 500 μm within the acrylic monolith. Placing the entire structure under vacuum evacuates most of the air from these cavities through a reservoir of liquid metal that covers a single inlet. Returning the assembly to atmospheric pressure pushes the metal from the reservoir into the cavities due to the pressure differential. This method enables filling of the closed internal cavities to create planar and curved conductive 3D geometries without leaving pockets of trapped air that lead to defects. An advantage of this technique is the ability to rapidly prototype 3D embedded antennas and other microwave components with metallic conductivity at room temperature using a simple process. Because the conductors are liquid, they also enable the possibility of manipulating the properties of such devices by flowing metal in or out of selected cavities. The measured electrical properties of fabricated devices match well to electromagnetic simulations, indicating that the approach described here forms antenna geometries with high fidelity. Finally, the capabilities and limitations of this process are discussed along with possible improvements for future work.

1. Introduction

Additive manufacturing (AM) processes are highly compelling for radio frequency (RF) and microwave electronic components, whose performance is largely dictated by their geometry and whose feature sizes are within the capabilities of modern 3D printers. For these devices, 3D printing offers additional degrees of freedom for RF design through configurations not possible with planar fabrication methods. For example, an electrically small conformal antenna formed by printing silver ink onto hemispherical surfaces supports a bandwidth that exceeds any linear or planar antenna with equivalent maximum dimension [1]. Moreover, in comparison to conventional manufacturing techniques, AM can reduce the number of processing steps and the resources required to build a prototype [2] and thus simplify the construction of custom geometries. For RF components such as waveguides, horn antennas and reflectors, these additively manufactured counterparts show the promise of being low cost [3,4], light-weight alternatives [5,6] while enabling corrugated [7], curved [8], or other complex conductive structures [9–11].

While complex dielectric geometries can be fabricated using a wide variety of AM processes [12], RF devices also require low-loss conductors. However, most AM techniques print non-conductive polymeric materials, and hence, must be followed by a separate metallization process. Surface metallization techniques such as electron beam evaporation [8] and sputtering [8,13] produce highly conductive layers but cannot readily coat internal surfaces. Other methods, such as electroless plating [5,7], can be used to metallize internal surfaces, but it is difficult to deposit metal layers more than a few microns thick, thereby limiting its use for components operating at the lower portion of the microwave band. Diffusion limitations also make it difficult to coat 'dead-end' capillaries evenly using electroless plating [14]. Alternatively, dispensing of conductive inks [1,15] or pastes can form finer metallic patterns on curved and planar printed surfaces. Although efforts have been directed towards developing highly conductive silver nanoparticle inks [15], they require a precise rheology for dispensing, followed by annealing at temperatures of at least 90 °C, that

* Corresponding author.
E-mail address: jacob.adams@ncsu.edu (J.J. Adams).
[1] These authors contributed equally.

https://doi.org/10.1016/j.addma.2017.10.012
2214-8604/

can lead to deformation or even melting of the 3D printed parts constructed using commercial high-resolution inkjet 3D printers [16]. Recently, silver suspension pastes have been used to metalize hollow cavities in order to fabricate simple electronic components such as resistors and LC resonant circuits [17]. Here, viscous pastes with silver-nanoparticle suspensions were injected into 3D printed microfluidic channels, that later solidify as the solvent evaporates during the ink curing process. The reduced volume on solidification or curing results in a lower packing density of the paste filled inside the cavities (and in extreme cases, cracking) that decreases the electrical conductivity [18]. Finally, these methods are incapable of creating reconfigurable electronic devices since the suspension dries after deposition, acting as a rigid conductor in the final device.

Gallium-based alloys such as EGaIn (an eutectic alloy of gallium and indium in 3:1 wt. ratio) pose an attractive substitute to conductive pastes because they are liquid at room temperature [19] with high conductivity of $\sim 3.4 \times 10^6$ *S/m* [20], low viscosity [21], and non-toxicity [22]. The fluidic nature of these alloys has recently been exploited to fabricate multi-axial Helmholtz coils [23] as well as reconfigurable [24,25] or flexible antennas such as a microstrip patch antenna [26], dipole antenna [27] and a planar inverted F-antenna (PIFA) [28] using an injection-based filling technique of relatively simple microfluidic channels constructed via 3D printing or soft lithography. Unlike simple RLC elements [17], antenna structures often consist of closed cavities without outlet paths for the metal. Some of them require wide planar surfaces and such geometries cannot be filled using direct injection without leaving internal voids [26]. Therefore, an alternative approach is needed to metallize RF components with closed cavities.

Here, we demonstrate a vacuum filling approach to embed liquid metals [19] in cavities constructed within a 3D printed acrylic monolith. The internal conductive structures consist of both straight and curved channels with high aspect ratios in addition to thin planes that constitute 3D printed RF transmission lines and antennas. We demonstrate the ability of our method to create a broad range of conductive shapes by printing a planar patch antenna with an embedded vertical coaxial transition and an axial mode helix antenna composed of curved and straight microchannels as well as a planar conducting ground. Furthermore, we examine the fabricated cylindrical channels to understand the accuracy of the internal dimensions produced using this technique. Combining this fabrication process with mechanical or electrochemical actuation [25,29] could lead to embedded microfluidic RF devices that are multi-functional and reconfigurable.

2. Materials and methods

Processes involving casting of molten metal have been traditionally used to obtain nano-scale metallic structures with high aspect ratios at elevated temperatures [30]. High pressure die-casting processes [31,32] typically use vacuum to avoid porosity in the casted part due to air entrapment. In case of metallizing 3D printed parts using liquid metal, a vacuum-driven filling process can similarly facilitate elimination of air voids without the need for repeated perturbation [33] in a hands-free manner. In addition, a room temperature filling process enables metallization of 3D printed soft polymeric and elastomeric substrates that have low heat distortion temperature. A high temperature filling process would be restricted to printed thermoplastics such as acrylonitrile butadiene styrene (ABS), polylactic acid (PLA), or polycarbonates printed using fused deposition modeling (FDM) [18,34] which is not suited for high resolution printing and requires complex support material removal procedures.

The proposed fabrication process is illustrated in Fig. 1. The CAD model of the antenna structure, designed with an EM simulator (HFSS, Ansys Inc.), is printed with a ProJet® 3500 HDMax [16] inkjet printing machine that uses VisiJet M3 Crystal® material – a photocurable dielectric resin used to encompass the liquid metal. M3 Crystal was selected due to its natural appearance, low warping during support material dissolution process, high mechanical strength and resistance to solvent exposure. The regions to be metalized are printed using a dissolvable wax-like support material (VisiJet S300®) to reinforce overhangs and free-standing geometries. The inkjet nozzles eject polymer droplets in the form of voxels that change its phase from a liquid to a gel, which is later flattened using a planarizer to form a thin film. The deposited layer is then UV-cured using a lamp with a wavelength of 365 nm. The wax material, when printed, solidifies instantaneously on the aluminum printpad as it is held at room temperature. These structures are printed at a layer thickness of 29 μm in the Ultra High Resolution (UHD) mode of the printer.

Once the part is printed, we hold the printpad in a freezer for two minutes to allow the mismatch in thermal expansion coefficient between the aluminum and the printed part to delaminate it from the printpad. The part is then transferred to a heated ultrasonic cleaning bath containing EZRinse-C® cleaning solution supplied by 3D Systems to dissolve away the printed wax supports at around 55 °C for two hours. The sample is then washed thoroughly with warm water to remove the remaining dissolved wax settled on the inner walls. Drain holes added at the edge of the antenna structure during the design stage simplify the removal of the support material and water. Finally, to evaporate any of the trapped water or surfactant, we transfer the part into a Thermo Scientific 280A vacuum oven held at 55 °C for 12 h.

Once the part is clean and dried as shown in Fig. 1a, a photocurable glue (Norland Optical Adhesive, NOA 63) seals the drain holes that assisted with the removal of the support materials. A snap-off reservoir (3D printed separately) is then mounted on the cleaned part and sealed as shown in Fig. 1b to aid the vacuum filling process. The reservoir is filled with a volume of EGaIn that is at least 30% more than expected to completely fill the antenna (avoiding entrance of air into the hollow cavities during vacuum-filling) and then kept inside a vacuum chamber at a pressure of −30 in. Hg relative to surrounding atmospheric pressure for 30 min. Returning the chamber to atmospheric pressure allows the liquid metal to rapidly fill the antenna cavities as illustrated in Fig. 1c (Appendix – Video A demonstrates this process for a scaled cross-sectional model of a patch antenna). The atmospheric pressure drives the metal into the cavities as shown in Fig. 1d. Finally, the reservoir is removed and replaced with a subminiature type A (SMA) connector that is affixed using NOA 63 to seal the device, as seen in Fig. 1e.

3. Antenna designs and measurements

3.1. Microstrip patch antenna

We first selected a common type of microstrip patch antenna to test the viability of the method. Patch antennas have wide and thin planar surfaces found in many types of antennas, yet these are difficult to fill uniformly by injecting metal due to the trapped air. To accurately design the device, we measured the complex permittivity of the VisiJet M3 Crystal® material using a resonant cavity method. Two cylindrical copper cavities were fabricated with the radius 1.1 cm and 3.825 cm and height equal to their radius. The changes in the resonance frequency and quality factor between an air-filled cavity and a cavity filled with M3 Crystal were observed to measure the dielectric constant ε_r' and loss tangent, respectively. Measurements of three different material samples led to an average relative dielectric constant of 2.96 (2.959 ± 0.003) and an average loss tangent of 0.047 (0.047 ± 0.0035) at 6 GHz. These values were

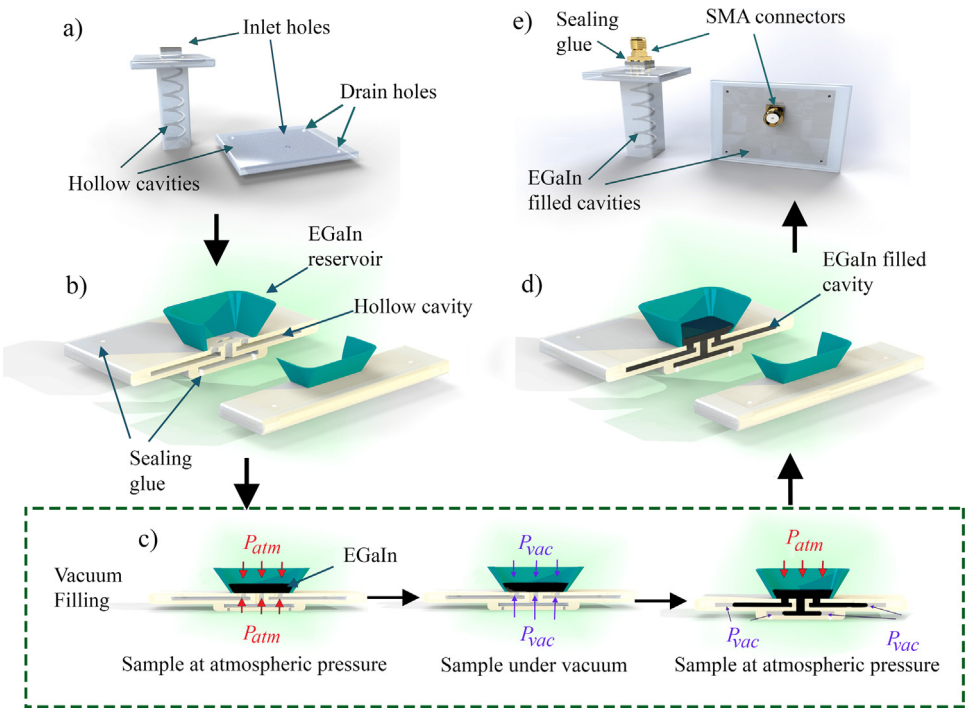

Fig. 1. An illustration depicting the fabrication process for liquid metal-filled 3D printed antenna geometries. a) 3D printed patch and helix antenna structures with sacrificial wax removed. b) Cross-sectional view of a patch antenna showing a snap-off reservoir for filling liquid metal and sealed drain holes. c) Filling liquid metal inside a patch antenna under vacuum. The air in the channel gets pulled through the liquid metal under vacuum. Upon returning to atmospheric pressure, the resulting pressure differential pushes the metal into the channels. d) Cross-sectional view of a liquid metal filled patch antenna, and e) Sealing the SMA connectors on the inlet holes to finish the antenna fabrication process.

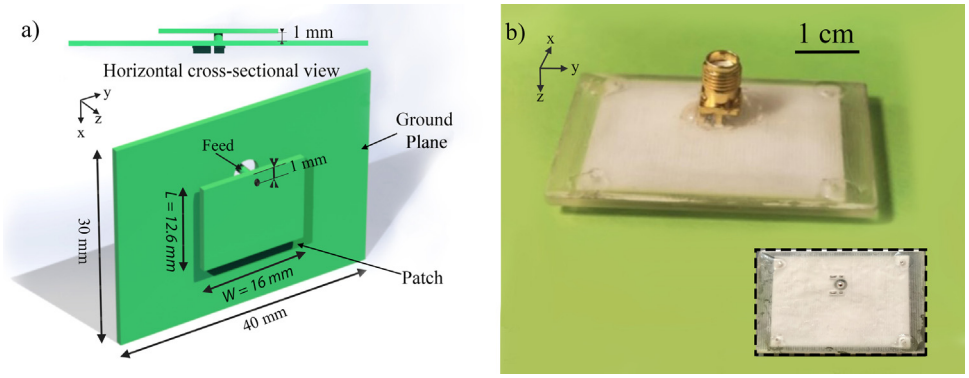

Fig. 2. a) The dimensions of the designed geometries for the metallic portion of the planar patch antenna b) Fabricated patch antenna showing the connector and ground plane and (inset) the liquid metal filled patch antenna sample before attaching the connector.

used in 3D electromagnetic simulations to select the patch antenna dimensions for operation at 6 GHz as shown in Fig. 2a.

The length of the rectangular patch was designed to be 12.6 mm and the width as 16 mm, placed at a height of 1 mm above the ground plane. A coaxial feed line provides a transmission path between the SMA connector and the rectangular patch wherein the inner coaxial conductor of diameter 1.3 mm opens directly to the patch element and the outer conductor of diameter 5.5 mm opens into the ground plane. This arrangement (cross-section illustrated in Fig. 1b) allows the entire geometry to be metalized through the coaxial inlet structure that also serves as the external RF feed port. As shown in Fig. 2a, an offset of 1 mm from the edge of the patch was used to match the input of the antenna [35] to a 50 Ω impedance. The fabricated microstrip patch sample is shown in Fig. 2b.

The measured reflection coefficient plot shown in Fig. 3a shows the operating frequency of the patch antenna sample as 5.97 GHz, and Fig. 3b shows the realized gain patterns in the E- and H-planes at this frequency. The realized gain of the antenna was measured to be 3.5 dBi while the simulated value was 2.9 dBi. Similarly, the simulated total efficiency of the patch antenna was 41% while that of the fabricated sample was 36%. Though the measured gain was slightly higher than simulated, the measured efficiency was lower. While these two quantities are linked and tend to vary in the same way, differences in the shape of the radiation pattern between measurement and simulation can cause them to differ as the beam becomes more or less directive.

Overall, both the reflection coefficient and the radiation pattern plots shown in Fig. 3 indicate a close alignment with the simulations. It is challenging to directly characterize the fidelity of the filled cavities, but the excellent agreement of the measured and simulated antenna properties confirms both the accuracy of the filled cavities and our characterization of the material properties of VisiJet M3 Crystal®.

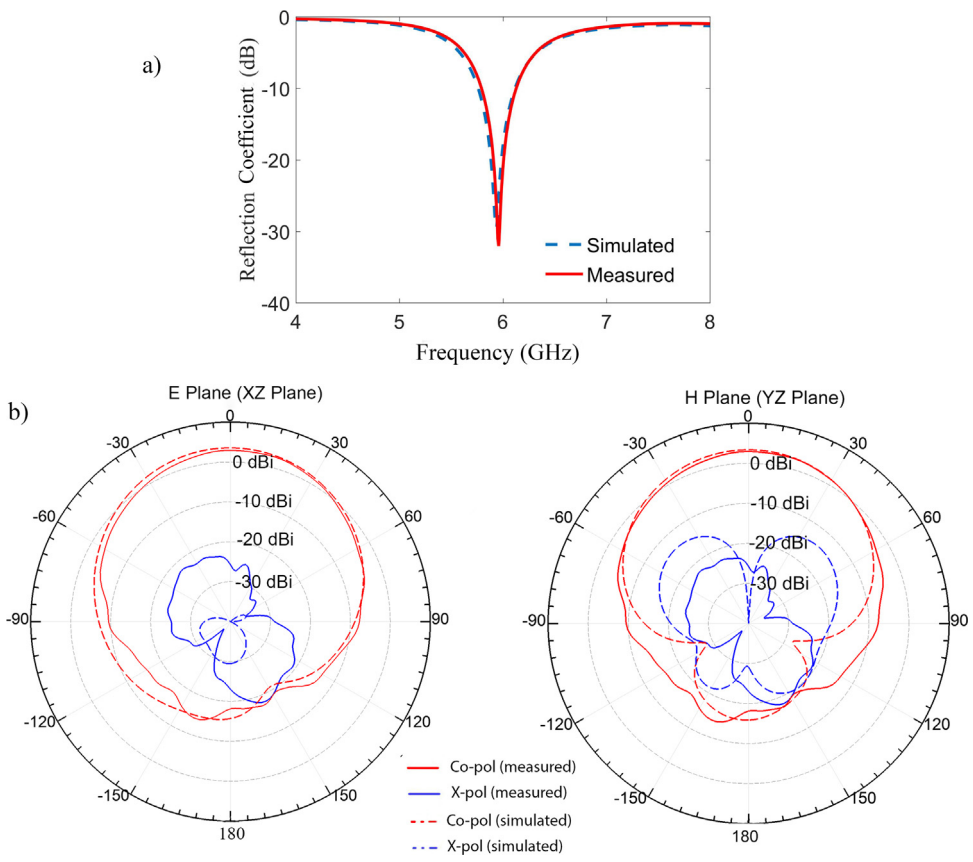

Fig. 3. a) The input reflection co-efficient response of the patch antenna sample, and b) the realized gain patterns for the patch antenna sample.

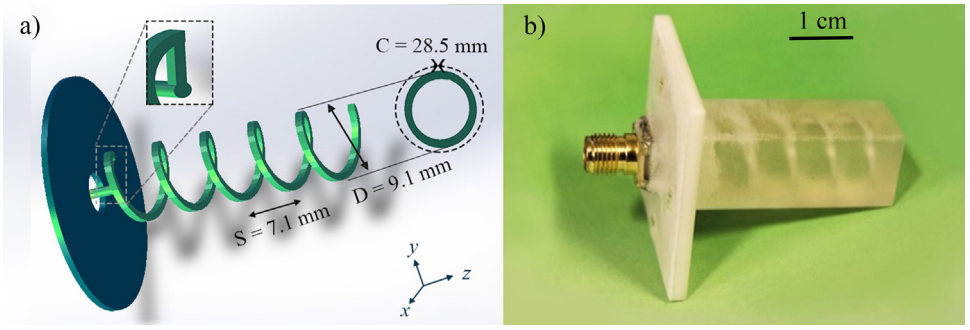

Fig. 4. a) The dimensions of the designed helical antenna and b) The fabricated helical antenna.

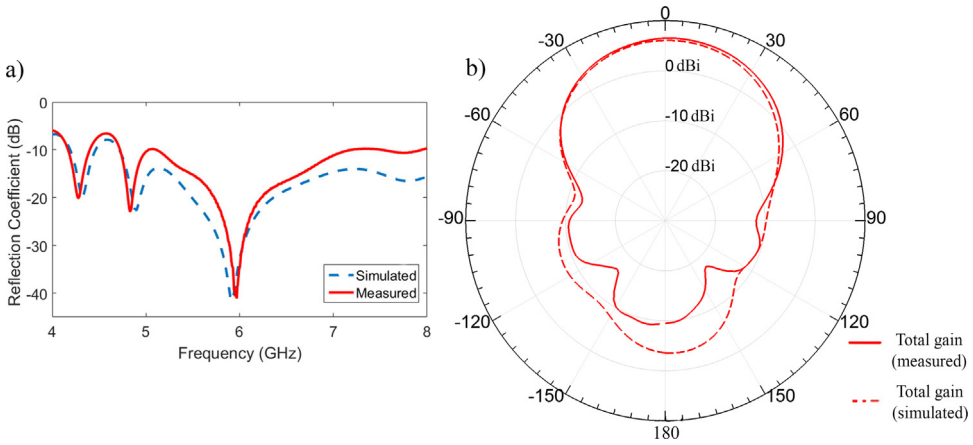

Fig. 5. a) The reflection coefficient measurements of the helical antenna, and b) The total gain pattern plot for helical antenna sample.

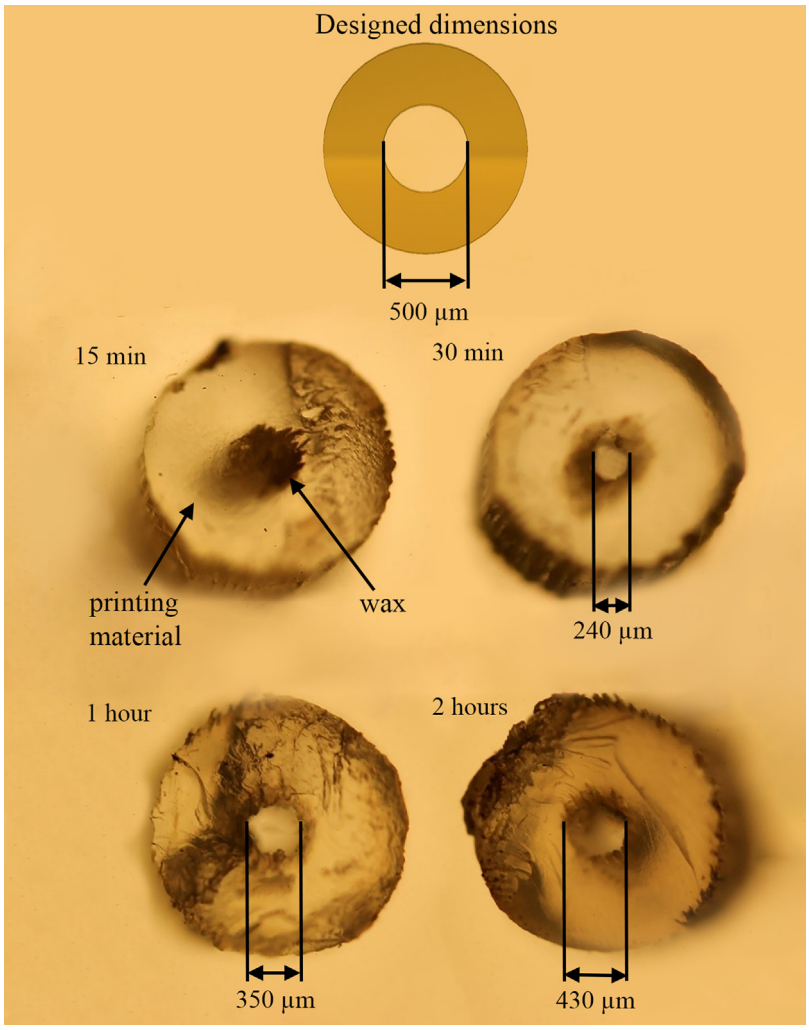

Fig. 6. Images depicting the time evolution of support material dissolution inside microchannels having an inner diameter of 500 μm.

3.2. Helical antenna

To demonstrate the ability of the vacuum filling method to metalize 3D geometries, a helical antenna radiating in the axial mode was designed using VisiJet M3 Crystal® with dimensions as shown in Fig. 4a. The pitch angle (α) of the 5 turn ($N = 5$) antenna was kept as 14° $\left[\alpha = \tan^{-1}\left(S/C\right)\right]$ and the diameter (D) as 9.1 mm for an operating frequency of 5.96 GHz. The input impedance of the helical antenna operating in axial mode with its circumference (C) equal to the wavelength (λ) is close to 140 Ω. This impedance was matched [36] to 50 Ω using a thin transmission line strip with width (w) as 0.74 mm at a height (h) of 0.53 mm above the ground plane as shown in Fig. 4a. The helical antenna has a ground plane and coaxial feed like the patch antenna discussed earlier.

Again, the agreement between the measured and simulated reflection coefficient and the radiation patterns (Fig. 5a & b) verify the ability of this method to accurately metalize curved hollow 3D structures. The measured total gain of the antenna (6.6 dBi) was again higher than the simulated gain (6 dBi). However, the axial ratio for the fabricated antenna was 2.2 dB as compared to the simulated axial ratio of 1.3 dB, which we attribute primarily to the drain holes and sealant placed asymmetrically at the top of the helix. The simulated total efficiency was 61% while the measured efficiency was slightly lower at 54%.

Table 1
Comparison of simulated efficiency of patch antenna using VisiJet M3 Crystal® and other engineered RF substrates.

Simulated Substrate Material	Loss Tangent (tanδ)	Total Efficiency (%)
VisiJet M3 Crystal®	0.047	40.5
FR4	0.018	61.8
Rexolite [37], Rogers Duroid 5880/5870 [38]	0.0005	91.1

4. Discussion

These measured samples indicate the ability to use the proposed vacuum filling process to fabricate planar, curved, and coaxial RF devices using 3D printing. While the performance of these printed devices is quite similar to conventional methods, it should be noted that the measured total efficiencies of the patch and helix (36% and 54%, respectively) are 2–3 dB lower than would be expected for a similar antenna made with typical materials (*e.g.*, copper and engineered RF composites).

Two factors can reduce the radiation efficiency – the lower conductivity of EGaIn [20] relative to copper and the high loss tangent of VisiJet M3 Crystal® material relative to engineered microwave substrates. To understand the significance of each of these factors, the loss tangent of the substrate was changed in simulation while keeping the rest of the geometry unchanged – including the resistive losses of the EGaIn. In Table 1, we observe that the total

efficiency increases to 91.1% when the loss tangent of VisiJet M3 Crystal® is reduced to 0.005. This suggests that dissipation in the dielectric is the dominant loss mechanism and that if a low loss tangent printable dielectric were readily available today, this process could produce antenna performance competitive with existing PCB fabrication processes.

However, conventional PCB materials and even common 3D printed materials with lower loss tangent, such as ABS and PLA, are not compatible with the PolyJet process, which enables the fine features and internal cavities required for embedded antennas using room temperature processing. Because the primary focus of this work is to demonstrate this new device topology and fabrication process, optimization of the antenna efficiency is not a key consideration here, but this study does indicate that there is a need for printable dielectrics that also exhibit favorable properties at microwave frequencies [37].

The antennas described here operate at 6 GHz. However, there are potential applications of this technology over a large range of frequencies, from hundreds of MHz to over 100 GHz. While scaling to lower frequencies is largely limited by printing area, a primary factor limiting the scaling to frequencies above 8 GHz is the ability to produce fine features. The print and flush process struggles to produce consistent lateral cavity dimensions when the critical feature size is below ~500 μm, despite the printer's vertical layer thickness of 29 μm. We printed a series of microfluidic channels with designed diameters varying from 200 μm to 1 mm and immersed them in the EZRinse-C® cleaning solution for periods varying from 15 min to 2 h. As shown in Fig. 6, in addition to a small amount of warping in samples, we observed that a microchannel designed with 500 μm inner diameter produced a maximum diameter of 430 μm after 2 h of submersion because of residual wax in the channel. Smaller diameter channels required longer submersion time to dissolve the wax. In fact, no dissolution was observed when the diameter was 200 μm. In addition, the pressure required to fill these channels scales inversely with the critical feature size as dictated by the Young-Laplace equation [19]. Hence, narrow cavities require large pressure gradients to fill completely. In addition, we observed the formation of voids that affect the antenna performance when cavity dimensions were less than 400 μm. Voids can also occur due to incomplete sealing of the drain holes or the reservoir prior to the vacuum filling process.

5. Conclusions

We have described a novel approach to fabricate complex 3D antennas for radio-frequency (RF) communication applications. The devices consist of liquid metal-filled cavities embedded in a printed acrylic substrate that offers the unique capability to simultaneously package the embedded RF device while producing complex conductive geometries. We metallized the inner cavities of the antennas – both planar and non-planar – using vacuum filling of a liquid metal alloy in a near room temperature process. The resulting devices are functional antennas with good impedance match and acceptable gain, in close agreement with electromagnetic simulations. Simulations indicate that these antennas exhibit reduced efficiency relative to conventional devices due to the poor loss characteristics of the printed acrylic. Thus, the device performance can be made competitive with conventional PCB fabrication methods by formulating printable dielectrics with improved loss characteristics. Additionally, the disparity between the lateral dimensions of the designed and printed geometries along with the pressure required to fill narrow cavities restricts the use of this approach for small feature sizes, but for frequencies below 8 GHz, this approach can be exploited to construct complex and potentially reconfigurable geometries. While not readily expanded to large-scale production, the proposed vacuum-filling method serves as a useful rapid prototyping and packaging technique for 3D RF devices, and which could in principle, be extended to elastomers to yield soft, flexible, or stretchable antennas.

Acknowledgements

The authors would like to thank National Science Foundation CMMI-1362284 for funding this research project as well as 3D Systems Corp. for providing the 3D printer along with the part and support materials for the antenna fabrication work. The authors would also like to acknowledge Dr. Shumin Wang and Joseph Merrill at Biomedical Research Imaging Center (BRIC) Small Animal Imaging at the University of North Carolina (UNC) School of Medicine for their help on micro-Computed Tomography (μCT) scanning work described in the Appendix A – Section A.

Appendix A.

Section A: Voids observed in a μCT Scan

An early model of the patch antenna printed using VisiJet M3 Crystal® was imaged using an eXplore speCZT CT120 scanner from General Electric (GE) as shown in Fig. A1a installed in the Biomedical Research Imaging Center (BRIC) at the University of North Carolina (UNC) School of Medicine.

The resolution of the scanner was ~6 μm and the image data shown in Fig. A1b was collected at the maximum tube voltage of 100 kVp and a tube current of 50 mA with a window width (WW) of 48,599, working level (WL) of 7254, nominal slice thickness (T) of 100 μm and an absolute slice location of 274.7 mm set in the viewing program that changes 100 μm at a time. The voxel size of the scanner was $0.0995 \times 0.0995 \times 0.0995\ mm^3$.

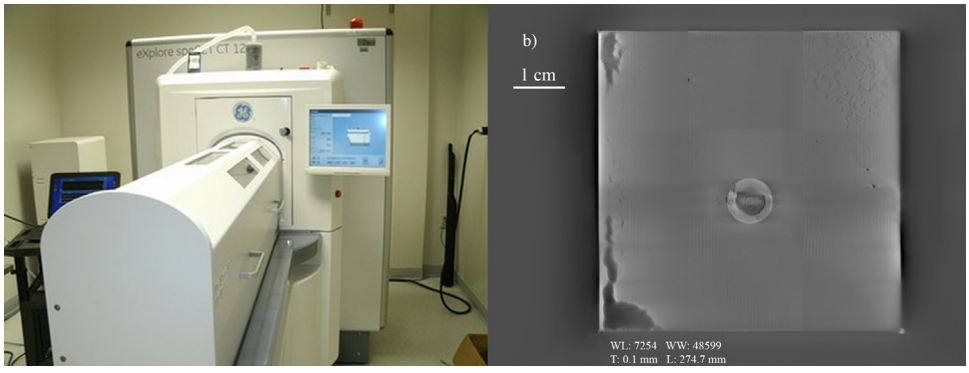

Fig. A1. a) GE eXplore speCZT CT120 Scanner at BRIC, and b) A μCT scan of an incompletely filled microstrip patch antenna illustrating presence of voids in the ground plane.

These initial prototypes of the antennas had visible internal voids that resulted in inconsistent and varying electrical performance. These voids were formed due to insufficient pressure required to fill cavities with small feature sizes (<500 μm), improper sealing of the EGaIn reservoir/drain holes during the vacuum filling procedure or due to leakage of liquid metal (filled inside the cavities) while attaching the SMA connector. An example of a scaled prototype of the microstip patch antenna with voids is demonstrated with the help of a reconstructed micro-Computed Tomography (μCT) image in Fig A1b. The pressure-related issues were mitigated by ensuring that the critical feature resolution of the channels in the cavity to be later metallized was least 500 μm ensuring a clear channel after the aforementioned wax dissolution process. Moreover, ensuring an air-tight sealing of the liquid metal reservoir using NOA 63 prevented air from re-entering the cavities during vacuum filling, avoiding visible voids. The samples presented in the main body use these improved fabrication procedures and do not show evidence of internal voids.

Appendix B. Supplementary data

Supplementary data associated with this article can be found, in the online version, at https://doi.org/10.1016/j.addma.2017.10.012.

References

[1] J.J. Adams, E.B. Duoss, T.F. Malkowski, M.J. Motala, B.Y. Ahn, R.G. Nuzzo, J.T. Bernhard, J.A. Lewis, Conformal printing of electrically small antennas on three-dimensional surfaces, Adv. Mater. 23 (2011) 1335–1340, http://dx.doi.org/10.1002/adma.201003734.

[2] I. Gibson, D. Rosen, B. Stucker, Additive Manufacturing Technologies, Springer, New York, 2015 http://link.springer.com/10.1007/978-1-4939-2113-3.

[3] P. Nayeri, M. Liang, R.A. Sabory-Garcıía, M. Tuo, F. Yang, M. Gehm, H. Xin, A.Z. Elsherbeni, 3D printed dielectric reflectarrays: low-cost high-gain antennas at sub-millimeter waves, IEEE Trans. Antennas Propag. 62 (2014) 2000–2008, http://dx.doi.org/10.1109/TAP.2014.2303195.

[4] M. Ahmadloo, P. Mousavi, A novel integrated dielectric-and-conductive ink 3D printing technique for fabrication of microwave devices, 2013 IEEE MTT-Int. Microw. Symp. Dig. MTT (2013) 1–3, http://dx.doi.org/10.1109/MWSYM.2013.6697669.

[5] E.G. Geterud, P. Bergmark, J. Yang, Lightweight waveguide and antenna components using plating on plastics, 2013 7th Eur. Conf. Antennas Propag. EuCAP (2013) 1812–1815.

[6] G.P.L. Sage, 3D printed waveguide slot array antennas, IEEE Access. 4 (2016) 1258–1265, http://dx.doi.org/10.1109/ACCESS.2016.2544278.

[7] P.T. Timbie, J. Grade, D. van der Weide, B. Maffei, G. Pisano, Stereolithographed MM-wave corrugated horn antennas, 2011 36th Int. Conf. Infrared Millim. Terahertz Waves IRMMW-THz (2011) 1–3, http://dx.doi.org/10.1109/irmmw-THz.2011.6104833.

[8] B.I. Wu, I. Ehrenberg, Ultra conformal patch antenna array on a doubly curved surface, 2013 IEEE Int. Symp. Phased Array Syst. Technol. (2013) 792–798, http://dx.doi.org/10.1109/ARRAY.2013.6731929.

[9] M. Liang, C. Shemelya, E. MacDonald, R. Wicker, H. Xin, 3-D printed microwave patch antenna via fused deposition method and ultrasonic wire mesh embedding technique, IEEE Antennas Wirel. Propag. Lett. 14 (2015) 1346–1349, http://dx.doi.org/10.1109/LAWP.2015.2405054.

[10] Amit Joe Lopes, Eric MacDonald, Ryan B. Wicker, Integrating stereolithography and direct print technologies for 3D structural electronics fabrication, Rapid Prototyp. J. 18 (2012) 129–143, http://dx.doi.org/10.1108/13552541211212113.

[11] P.I. Deffenbaugh, T.M. Weller, K.H. Church, Fabrication and microwave characterization of 3-D printed transmission lines, IEEE Microw. Wirel. Compon. Lett. 25 (2015) 823–825, http://dx.doi.org/10.1109/LMWC.2015.2495184.

[12] D.P. Parekh, D. Cormier, M.D. Dickey, Multifunctional printing incorporating electronics into 3D parts made by additive manufacturing, Addit. Manuf. (2015) 215.

[13] F. Cai, W.T. Khan, J. Papapolymerou, A low loss X-band filter using 3-D Polyjet technology, 2015 IEEE MTT- Int. Microw. Symp. (2015) 1–4, http://dx.doi.org/10.1109/MWSYM.2015.7166895.

[14] E.K. Yung, L.T. Romankiw, R.C. Alkire, Plating of copper into through-holes and vias, J. Electrochem. Soc. 136 (1989) 206–215, http://dx.doi.org/10.1149/1.2096587.

[15] S.B. Walker, J.A. Lewis, Reactive silver inks for patterning high-conductivity features at mild temperatures, J. Am. Chem. Soc. 134 (2012) 1419–1421, http://dx.doi.org/10.1021/ja209267c.

[16] 3D Systems ProJet® 3500 HDMax URL:http://www.3dsystems.com/3d-printers/professional/projet-3500-hdmax.

[17] S.-Y. Wu, C. Yang, W. Hsu, L. Lin, 3D-printed microelectronics for integrated circuitry and passive wireless sensors, Microsyst. Nanoeng. 1 (2015) 15013, http://dx.doi.org/10.1038/micronano.2015.13.

[18] I.T. Nassar, T.M. Weller, H. Tsang, A 3-D printed miniaturized log-periodic dipole antenna, IEEE Antennas Propag. Soc. Int. Symp. APSURSI (2014) 11–12, http://dx.doi.org/10.1109/APS.2014.6904337.

[19] M.D. Dickey, R.C. Chiechi, R.J. Larsen, E.A. Weiss, D.A. Weitz, G.M. Whitesides, Eutectic gallium-indium (EGaIn): a liquid metal alloy for the formation of stable structures in microchannels at room temperature, Adv. Funct. Mater. 18 (2008) 1097–1104, http://dx.doi.org/10.1002/adfm.200701216.

[20] D. Zrnic, D.S. Swatik, Resistivity and surface tension of the eutectic alloy of gallium and indium, J. Common Met. 18 (1969) 67–68.

[21] J.N. Koster, Directional solidification and melting of eutectic gain, Cryst. Res. Technol. 34 (1999) 1129–1140, http://dx.doi.org/10.1002/(SICI)1521-4079(199911)34:9<1129:AID-CRAT1129>3.0.CO;2-P.

[22] D.R. Lide, CRC Handbook of Chemistry and Physics, Internet Version 2007, Taylor Francis, Boca Raton FL, 2007, pp. 87.

[23] L. Li, R. Abedini-Nassab, B.B. Yellen, Monolithically integrated helmholtz coils by 3-dimensional printing, Appl. Phys. Lett. 104 (2014), http://dx.doi.org/10.1063/1.4885441.

[24] Pan, Liquid Metal Reconfigurable Antennas, 2017 http://oaktrust.library.tamu.edu/bitstream/handle/1969.1/158079/PAN-THESIS-2016.pdf?sequence=1&isAllowed=y.

[25] M. Wang, C. Trlica, M.R. Khan, M.D. Dickey, J.J. Adams, A reconfigurable liquid metal antenna driven by electrochemically controlled capillarity, J. Appl. Phys. 117 (2015) 194901, http://dx.doi.org/10.1063/1.4919605.

[26] G.J. Hayes, Ju-Hee So, A. Qusba, M.D. Dickey, G. Lazzi, Flexible liquid metal alloy (EGaIn) microstrip patch antenna, IEEE Trans. Antennas Propag. 60 (2012) 2151–2156, http://dx.doi.org/10.1109/TAP.2012.2189698.

[27] J.-H. So, J. Thelen, A. Qusba, G.J. Hayes, G. Lazzi, M.D. Dickey, Reversibly deformable and mechanically tunable fluidic antennas, Adv. Funct. Mater. 19 (2009) 3632–3637, http://dx.doi.org/10.1002/adfm.200900604.

[28] M. Cosker, F. Ferrero, L. Lizzi, R. Staraj, J.M. Ribero, 3D flexible antenna realization process using liquid metal and additive technology, 2016 IEEE Int. Symp. Antennas Propag. APSURSI (2016) 809–810, http://dx.doi.org/10.1109/APS.2016.7696113.

[29] M.R. Wang, C. Trlica, M.D. Dickey, J.J. Adams, Pump-free feedback control of a frequency reconfigurable liquid metal monopole, 2015 IEEE Int. Symp. Antennas Propag. Usn. Natl. Radio Sci. Meet. (2015) 2223–2224, http://dx.doi.org/10.1109/APS.2015.7305500.

[30] C.-G. Kuo, H. Chang, J.-H. Wang, Fabrication of ZnO nanowires arrays by anodization and high-vacuum die casting technique, and their piezoelectric properties, Sensors 16 (2016) 431, http://dx.doi.org/10.3390/s16040431.

[31] X.P. Niu, B.H. Hu, I. Pinwill, H. Li, Vacuum assisted high pressure die casting of aluminium alloys, J. Mater. Process. Technol. 105 (2000) 119–127, http://dx.doi.org/10.1016/S0924-0136(00)00545-8.

[32] A.A. Luo, Magnesium casting technology for structural applications, J. Magnes. Alloys. 1 (2013) 2–22, http://dx.doi.org/10.1016/j.jma.2013.02.002.

[33] A. Fassler, C. Majidi, 3D structures of liquid-phase GaIn alloy embedded in PDMS with freeze casting, Lab Chip 13 (2013) 4442–4450, http://dx.doi.org/10.1039/C3LC50833A.

[34] S.H. Masood, K. Mau, W.Q. Song, Tensile properties of processed FDM polycarbonate material, Mater. Sci. Forum 654–656 (2010) 2556–2559, http://dx.doi.org/10.4028/www.scientific.net/MSF.654-656.2556.

[35] C. Balanis, Antenna Theory: Analysis and Design, 3rd edition, John Wiley & Sons, Ltd, 2005 https://www.academia.edu/11205305/Antenna_Theory_Analysis_and_Design_3rd_Edition_by_Balanis.

[36] J. Kraus, A 50-ohm input impedance for helical beam antennas, IEEE Trans. Antennas Propag. 25 (1977) 913, http://dx.doi.org/10.1109/TAP.1977.1141687.

[37] M. Lis, M. Plaut, A. Zai, D. Cipolle, J. Russo, J.A. Lewis, T. Fedynyshyn, Polymer dielectrics for 3D-printed RF devices in the ka band, Adv. Mater. Technol. (2016).

[38] Rogers Corp., Rogers Duroid 5880 URL: http://www.rogerscorp.com/documents/606/acs/RT-duroid-5870-5880-Data-Sheet.pdf.